RECENT RESULTS FROM THE ZEUS EXPERIMENT

WESLEY H. SMITH (ON BEHALF OF THE ZEUS COLLABORATION)

Physics Dept., University of Wisconsin, Madison, WI 53706 USA E-mail: wsmith@hep.wisc.edu

A summary of recent results from ZEUS is presented. New ZEUS results from HERA-1 data include Structure Functions, QCD fits, analysis of hadronic final states, precision measurements of α_s , production of heavy flavor mesons and baryons and studies of diffraction. Results from the new HERA-II running include the measurement of the cross section for polarized charged current events and charm events tagged with the new ZEUS vertex detector.

1 Introduction

There are new ZEUS results on total neutral and charged current differential cross sections, structure functions, and their QCD fits. Analyses of the hadronic final states in these data have produced several precision measurements of α_s and have been used to test new NLO QCD calculations.

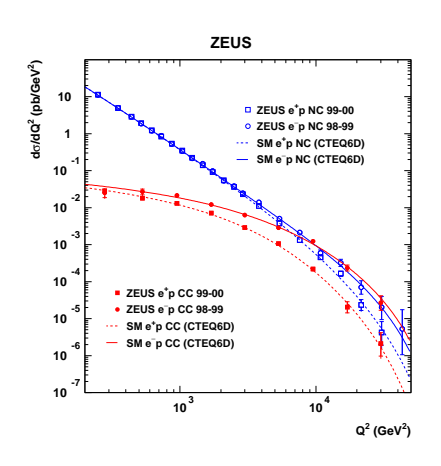
ZEUS data show evidence for pentaquark baryons with strangeness. Precision measurements of charm production in DIS may now be used to check NLO calculations and constrain the gluon content of the proton. Measurements of B production in photoproduction and DIS are showing improving agreement with NLO QCD. Electroproduction of ϕ and J/ ψ mesons show consistency with VMD and Regge phenomenology as well as with pQCD. Diffractive charm production can now begin to discriminate amongst diffractive parton distribution functions.

Following the upgrade to HERA-II, the ZEUS detector turned on with new microvertex and forward tracking detectors. In 2004, HERA achieved longitudinal polarization of $>50\,\%$ and has begun to deliver luminosities approaching the required rate to reach the luminosity goal. Physics results from the beginning of the HERA-II luminosity running with 33 % polarized positrons show that the ZEUS detector upgrades are working well.

These ZEUS results are discussed below and presented in greater detail in the individual contributions in these proceedings.

2 Cross Sections, Structure Functions and QCD fits

ZEUS has measured the Charged and Neutral Current cross sections for collisions of positrons and electrons on protons from the full HERA-I data sample. Figure 1 shows the NC and CC cross sections as a function of Q^2 for e^+p and e^-p scattering as measured by the ZEUS [2] experiment. The ZEUS measurements are in a good agreement with expectations of the Standard Model (SM), calculated with the CTEQ6D [3] parameterization of parton distribution functions (PDFs) in the



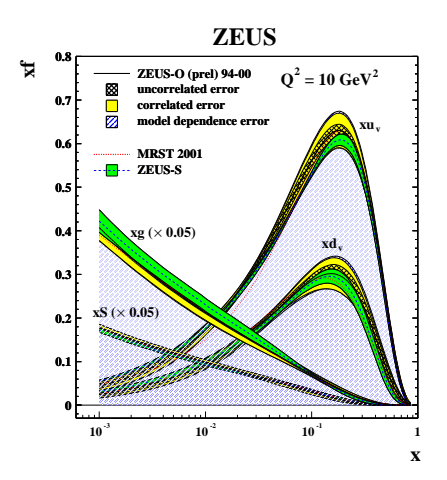


Figure 1. The NC and CC cross sections versus Q^2 for e^+p and e^-p interactions.

Figure 2. New ZEUS-only PDFs fit using high- Q^2 data.

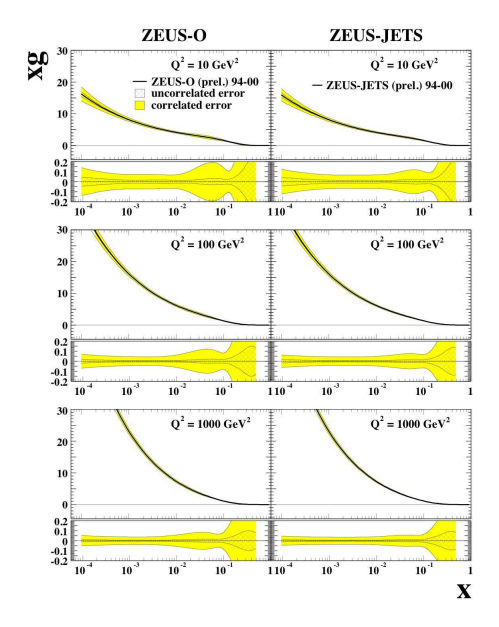
proton.

Figure 2 shows results of the latest structure function fit based on ZEUS data alone from the full HERA-I sample (ZEUS-O). The addition of data used in the fit up to a Q^2 of 30,000 GeV² reduces the need for fixed target data and sum rules to constrain the fit for x > 0.05. There is good agreement between these new fits and the previous ZEUS fits (ZEUS-S) from the 1994-1998 data sample, which made more use of fixed target data, and with the MRST 2001 PDF [8].

3 Hadronic Final States

The ZEUS collaboration has recently developed a rigorous and consistent technique for including jets in QCD fits. Figure 3 shows the effect of combining inclusive DIS jet data and high E_T dijet photoproduction data into the ZEUS QCD fits. The figure shows the ZEUS-only gluon fit with and without the jet data included in the fit. The jet data constrains the medium-x gluon distribution, providing improved precision on the gluon for 0.01 < x < 0.1.

Event shape variables have been measured in the current region of the Breit frame for NC DIS events. The Q-dependence of the means and distributions of the shape variables has been compared with a model based on fixed-order plus next-to-leading-logarithm perturbative calculations and the Dokshitzer-Webber [5] non-perturbative corrections ("power corrections"). The event shapes examined and displayed in Fig. 4 include thrust with respect to the thrust (T_T) and γ (T_{γ}) axes, broadening (B_{γ}) , jet mass (M^2) and particle pair correlations (C). The power corrections introduce the parameter $\bar{\alpha}_0$ to describe the non-perturbative effects: $\langle F \rangle = \langle F \rangle_{NLO} + \langle F (\bar{\alpha}_0) \rangle_{POW}$. The differential distributions are fit with the combination of NLO QCD with power corrections and NLL resummation [6], producing $\alpha_s \simeq 0.118$, and $\bar{\alpha}_0 \simeq 0.5$. The resummation extends the fit range and



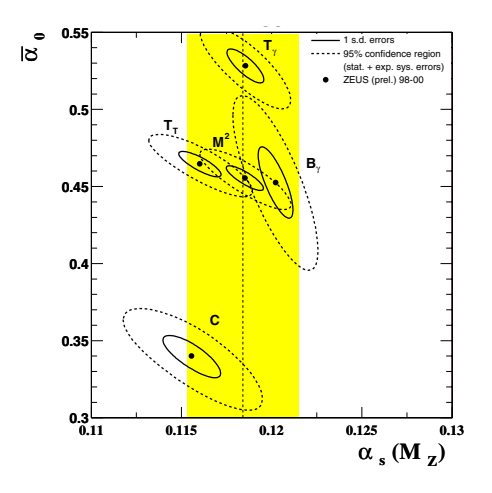


Figure 3. ZEUS data only gluon QCD fits with (right) and without (left) ZEUS inclusive DIS and high E_T dijet photoproduction data incorporated.

Figure 4. α_s vs. $\bar{\alpha}_0$ derived from event shape variables measured in the current region of the Breit frame.

yields consistent values of α_s and $\bar{\alpha}_0$ for $T_{\gamma}, T_T, B_{\gamma}$, and M^2 , with C displaying some disagreement which depends on the fit range used.

The integrated jet shape, $\psi(r)$, is the fraction of the jet transverse energy that lies inside a cone in the $\eta-\varphi$ plane of radius r concentric with the jet axis while the mean integrated jet shape, $\langle \psi(r) \rangle$, is defined as the averaged fraction of the jet transverse energy inside the cone. Measurements of the mean integrated jet shape in DIS have been used to extract a value of $\alpha_s(M_Z)$ by comparing to the NLO QCD predictions of DISENT [12] as a function of $E_T^{\rm jet}$. The calculations reproduce the measured observables well, demonstrating the validity of the description of the internal structure of jets by pQCD. The values of $\alpha_s(M_Z)$ as determined from the measured $\langle \psi(r=0.5) \rangle$ in each region of $E_T^{\rm jet}$ are shown in Fig. 5. The value of $\alpha_s(M_Z)$ as determined by fitting the NLO QCD calculations to the measured mean integrated jet shape $\langle \psi(r=0.5) \rangle$ for $E_T^{\rm jet} > 21$ GeV is $\alpha_s(M_Z) = 0.1176 \pm 0.0009$ (stat.) $^{+0.0091}_{-0.0026}$ (exp.) $^{+0.0091}_{-0.0072}$ (th.). This value is in good agreement with the current world average. Comparisons of several ZEUS measurements of $\alpha_s(M_Z)$ with the current world average are shown in Fig. 6. ZEUS is performing precision jet physics with systematic errors at the level of 2%.

ZEUS has measured the differential dijet and trijet cross sections in neutral current DIS for $10 < Q^2 < 5000~GeV^2$ with high precision. These cross sections have been measured as functions of the jet transverse energy in the Breit Frame, $E_{T,B}^{jet}$, η_{LAB}^{jet} , and Q^2 for jets with $E_{T,B}^{jet} > 5~\text{GeV}$ and $-1 < \eta_{LAB}^{jet} < 2.5$. Events

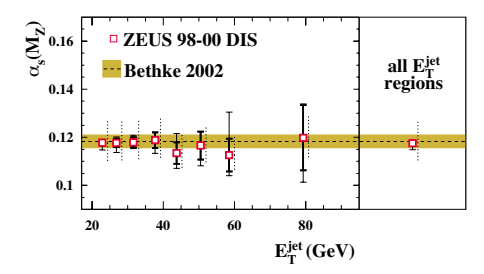


Figure 5. The section of the plot on the right shows the $\alpha_s(M_Z)$ values determined from the QCD fit of the measured integrated jet shape $\langle \psi(r=0.5) \rangle$ in different $E_T^{\rm jet}$ regions (squares). The part on the right shows the combined value of $\alpha_s(M_Z)$ obtained using all the $E_T^{\rm jet}$ regions (square). In both plots, the inner error bars represent the statistical uncertainties of the data. The outer error bars show the statistical and systematic uncertainties added in quadrature. The dotted vertical bars represent the theoretical uncertainties

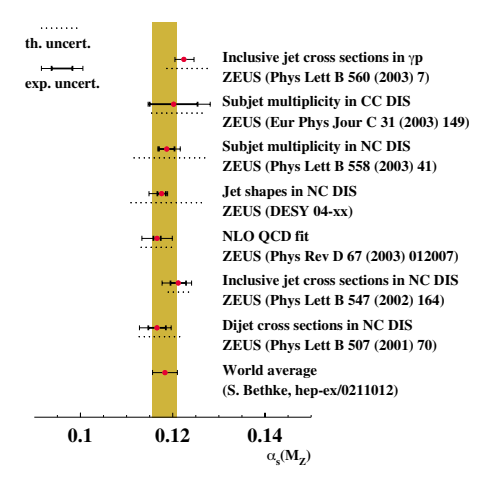


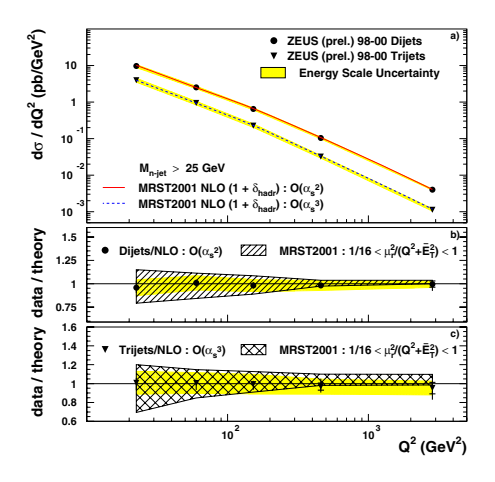
Figure 6. $\alpha_s(M_Z)$ values determined from ZEUS jet measurements, and QCD fits to ZEUS structure functions compared with the world average.

with two (three) or more jets were required to have the invariant mass of the two (three) highest $E_{T,B}^{jet}$ jets to be greater than 25 GeV to enable comparison with reliable NLO calculations.

The differential dijet and trijet cross sections as functions of Q^2 are presented in Fig. 7. The largest uncertainty in the data is due to absolute energy scale of the calorimeter. The cross sections are compared with the NLOJET [7] program using the MRST2001 [8] PDFs and corrected for hadronization effects using the Lepto [9] 6.5 program. Uncertainties due to terms beyond NLO were estimated by varying both μ_R and μ_F between $(\bar{E}_T^2 + Q^2)$ and $(\bar{E}_T^2 + Q^2)/16$. The data is well described by the NLO QCD prediction. The renormalization scale error grows larger at low Q^2 .

Figure 8 shows the ratio of trijet to dijet cross sections as a function of Q^2 . The correlated systematic and renormalization scale uncertainties cancel in this ratio. The agreement between the data and the NLO predictions is good within the uncertainties (experimental $\sim 5 \%$, theoretical $\sim 7 \%$), which are substantially reduced from those of the dijet and trijet cross sections alone and should be able to yield another precise measurement of $\alpha_s(M_Z)$.

In the DGLAP formalism, the parton cascade that results from the hard scattering of the virtual photon with a parton from the proton is ordered in parton virtuality. This ordering along the parton ladder implies an ordering in transverse energy of the partons, with the parton participating in the hard scatter having the highest transverse energy. In the BFKL formalism there is no strict ordering in virtuality and transverse energy. Since the partons emitted at the bottom of the ladder are closest in rapidity to the outgoing proton, they are manifested as forward jets. BFKL evolution predicts that a larger fraction of small x events will contain



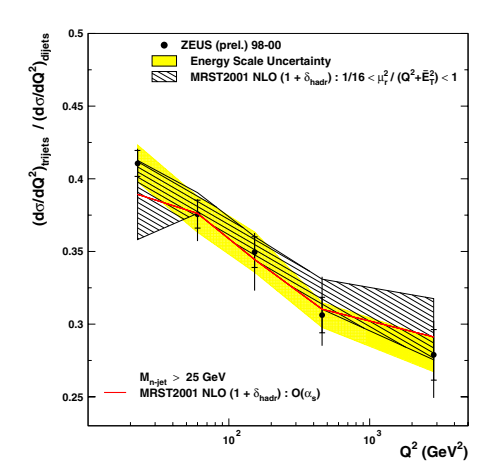


Figure 7. a) The inclusive dijet and trijet cross sections as functions of Q^2 . the predictions of NLO pQCD is compared to the data. b) and c) show the ratio of data over predictions. The hashed band represents the renormalization scale uncertainty of the QCD calculation.

Figure 8. The ratio of inclusive trijet over dijet cross section as a function of Q^2 . The predictions of NLO pQCD are compared to the data. The hashed band represents the renormalization scale uncertainty of the QCD calculation.

high E_T forward jets than is predicted by DGLAP [10].

ZEUS has performed measurements of the DIS differential inclusive forward jet cross sections in the lab frame with the specific restrictions $\cos \gamma_h < 0$ (where γ_h is the angle that defines the average direction of the hadronic system) to remove single jets, $2 < \eta_{jet} < 3$ to select forward jets and $0.5 < \frac{E_{T,jet}^2}{Q^2} < 2$ to limit the Q^2 evolution of the particles on the parton ladder. This phase space region is where events exhibiting BFKL effects are expected to be dominant. The measurements are presented in Fig. 9. The predictions of ARIADNE [11] describe the data well, whereas the predictions of Lepto [9] fail in all distributions. The ARIADNE program uses the Color Dipole Model, which treats gluons emitted from quark-antiquark (diquark) pairs as radiation from a color dipole between two partons. This results in partons that are not ordered in their transverse momenta.

The measurements are also compared with QCD predictions evaluated using the event generator DISENT [12]. The calculation describes the measurement as a function of x_{Bj} at high values, but underestimates the data in the low x_{Bj} region by nearly a factor of two. In this region there is a large renormalization uncertainty, an indication of the importance of higher orders.

QCD predicts an asymmetry in the azimuthal distribution of hadrons around the virtual photon direction in the hadronic center of mass frame (HCM) as manifested in the distribution of the angle between the hadron production plane and the electron scattering plane. QCD also predicts that this azimuthal asymmetry will evolve in η^{HCM} because the contributions of the originating QCD-Compton and Boson Gluon fusion processes vary with η^{HCM} . Figure 10 shows the ZEUS result for the η^{HCM} dependence of this asymmetry from a new analysis using energy

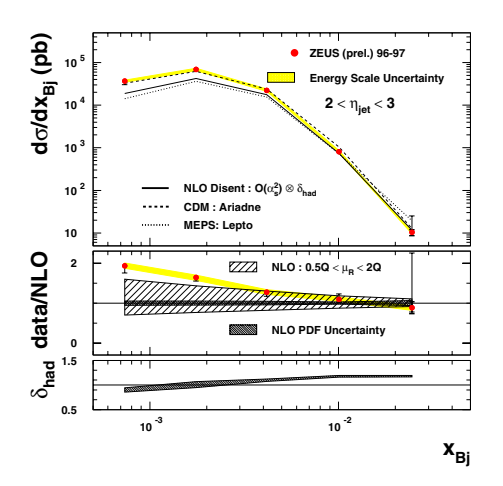


Figure 9. Measured differential cross section (dots) in the forward BFKL phase space for inclusive jet production in NC DIS with $E_{T,jet} > 6$ GeV and $2 < \eta_{jet} < 3$ in the kinematic region defined by $Q^2 > 25~GeV^2$, y > 0.04 and $\cos \gamma_h < 0$ as a function of x_{Bj} . The lower section of each plot shows the hadronisation correction factor applied to the QCD calculations.

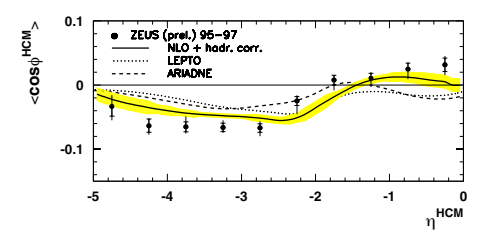


Figure 10. η^{HCM} dependence of the azimuthal asymmetry of ZEUS DIS data using energy flow objects in the hadronic center of mass frame compared with LO MCs and a NLO calculation.

flow objects in the hadronic center of mass frame. This analysis includes charged and neutral hadrons where previous analyses ony included charged tracks. It also enhances the contributions from hard partons since these energy flow objects are weighted by energy. The data are compared with LO MC (LEPTO and ARIADNE) and NLO calculations corrected to the hadron level by the LO MC. The NLO effects are not negligible and provide better agreement with experimental data.

4 Heavy Flavors

ZEUS has performed a search for pentaquarks in K_S^0 p (\bar{p}) decay channel [13]. The analysis used deep inelastic scattering events measured with exchanged-photon virtuality $Q^2 \geq 1 \text{ GeV}^2$. The data sample corresponded to an integrated luminosity of 121 pb⁻¹. The charged tracks were selected in the central tracking (CTD) with $p_T \geq 0.15 \text{ GeV}$ and $|\eta| \leq 1.75$, restricting this study to a region where the CTD track acceptance and resolution are high.

Figure 11 shows the K_S^0 p (\bar{p}) invariant mass for $Q^2>20~{\rm GeV}^2$, as well as for the K_S^0 p and K_S^0 \bar{p} samples separately (shown as inset). The data is above the Ariadne Monte Carlo model near 1470 MeV and 1522 MeV, with a clear peak at 1522 MeV.

To extract the signal seen at 1522 MeV, the fit was performed using a background function plus two Gaussians. The first Gaussian, which significantly improves the fit at low masses, may correspond to the unestablished PDG $\Sigma(1480)$. The peak position determined from the second Gaussian was

 $1521.5 \pm 1.5 ({\rm stat.})^{+2.8}_{-1.7} ({\rm syst.})$ MeV. It agrees well with the measurements by HER-MES, SVD and COSY-TOF for the same decay channel [14]. If the width of the Gaussian is fixed to the experimental resolution, the extracted Breit-Wigner width of the signal is $\Gamma = 8 \pm 4 ({\rm stat.})$ MeV.

The number of events ascribed to the signal by this fit was 221 ± 48 . The statistical significance, estimated from the number of events assigned to the signal by the fit, was 4.6σ . The number of events in the $K_S^0 \bar{p}$ channel was 96 ± 34 . It agrees well with the signal extracted for the $K_S^0 p$ decay mode. If the observed signal corresponds to the pentaquark, this provides the first evidence for its antiparticle with a quark content of $\bar{u}\bar{u}d\bar{d}s$.

ZEUS has measured the open-charm contribution, $F_2^{c\bar{c}}$, to the proton structure-function F_2 . This final HERA-I result is based on 5500 D^* , providing 31 additional data points over the previous ZEUS result [17] and increasing the range up to $Q^2 = 500 \text{ GeV}^2$. The data for $F_2^{c\bar{c}}$ as a function of x for fixed Q^2 are shown in Figure 12 to be consistent with previous measurements from H1 [16] and ZEUS [17] and with the recent ZEUS NLO fit [15]. The data rise with increasing Q^2 , with the rise becoming steeper at lower x, demonstrating the property of scaling violation in charm production. The uncertainty on the theoretical prediction is that from the PDF fit propagated from the experimental uncertainties of the fit data. At the lowest Q^2 , the uncertainty in the data is comparable to the PDF uncertainty shown. This implies that the double-differential cross sections could be used as an additional constraint on the gluon density in the proton.

ZEUS has measured beauty photoproduction in events with two jets and a muon, for $Q^2 < 1~{\rm GeV}^2$ [19]. These events have been shown to agree with NLO QCD predictions based on the FMNR [20] program. This NLO QCD prediction was used to extrapolate the cross section for dijet events with a muon to the inclusive b-quark cross section. The b-quark differential cross section was measured as a function of the quark transverse momentum, $d\sigma(ep \to bX)/dp_T^b$, for b-quark pseudorapidity in the laboratory frame $|\eta^b| < 2$. The result, shown in Figure 13, is consistent with the previous ZEUS result from semi-leptonic B decays into electrons [18] translated into the b-quark cross section for $p_T^b > p_T^{\rm min} = 5~{\rm GeV}$ and $|\eta^b| < 2$, converted to a differential cross section using the NLO prediction and plotted at the average b-quark transverse momentum. Beauty photoproduction in ep collisions is reasonably well described by NLO QCD.

ZEUS has also measured the b cross section in DIS events with at least one hard jet in the Breit frame $(E_T^{Breit}>6GeV)$ together with a muon and electron for photon virtualities $Q^2>2{\rm GeV}^2$, as well as from events with a muon and a D*. These measurements have been compared with an NLO QCD calculation in the HVQDIS program [21]. Figure 14 compares the cross sections from these measurements and the photoproduction measurements in various kinematic regions shown with the NLO QCD calculation. While, as mentioned above, the photoproduction measurements are in good agreement with the NLO QCD calculation, the DIS measurements, although in general consistent with the NLO QCD calculation, are about two standard deviations above the NLO QCD calculation at low values of Q^2 , Bjorken x and muon transverse momentum, and high values of jet transverse energy and muon pseudorapidity.

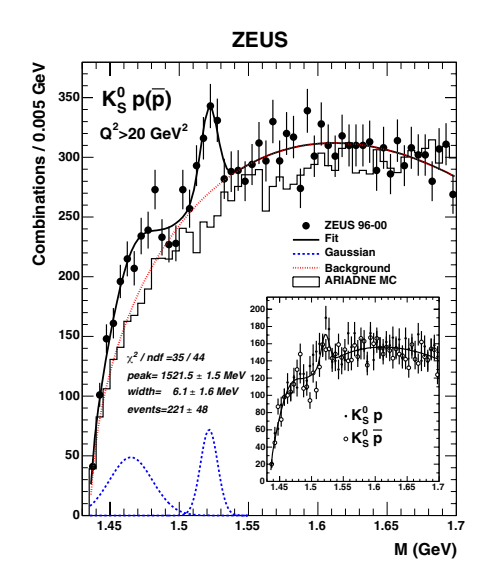


Figure 11. Invariant-mass spectrum for the K_S^0 p (\bar{p}) channel for $Q^2>20~{\rm GeV}^2$. The solid line is the result of a fit to the data using the threshold background plus two Gaussians. The dashed lines show the Gaussian components, while the dotted line indicates background. The prediction of the Monte Carlo simulation is normalized to the data in the mass region above 1650 MeV. The inset shows the K_S^0 \bar{p} (open circles) and the K_S^0 p (black dots) candidates separately, compared to the result of the fit to the combined sample scaled by a factor of 0.5.

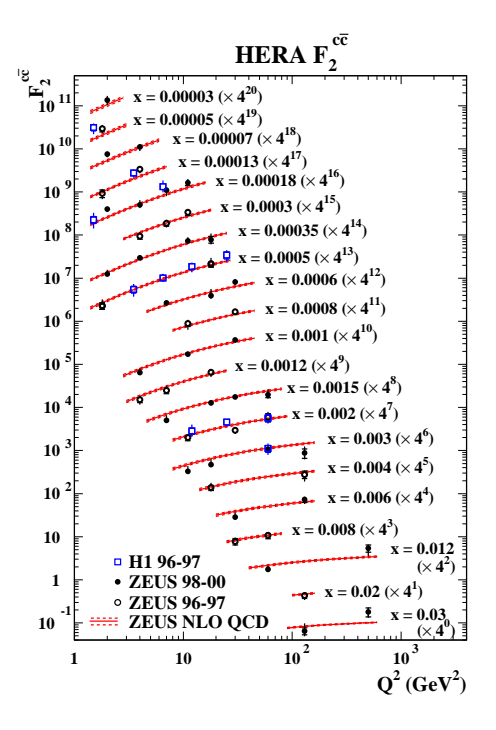


Figure 12. The measured $F_2^{c\bar{c}}$ as a function of Q^2 for fixed x compared with previous H1 and ZEUS measurements and the predictions from the ZEUS NLO QCD fit.

5 Diffraction and Vector Meson Production

ZEUS has measured the exclusive electroproduction of J/ψ mesons, $ep \to eJ/\psi \ p$, for photon virtualities in the ranges $0.15 < Q^2 < 0.8 \ {\rm GeV}^2$ and $2 < Q^2 < 100 \ {\rm GeV}^2$, for photon-proton center-of-mass energies in the range $30 < W < 220 \ {\rm GeV}$. The cross section of the process $\gamma^* \ p \to J/\psi \ p$ measured for $|t| < 1 \ {\rm GeV}^2$, but extrapolated to the full t range, rises with W as $\sigma \propto W^\delta$, with a slope parameter δ of about 0.7. This parameter does not change significantly with Q^2 and is consistent with that observed in J/ψ photoproduction. The cross section at $W=90 \ {\rm GeV}$ and over the whole Q^2 range is described by the function $\sigma \propto (Q^2 + M_{J/\psi}^2)^{-n}$, with $n=2.44\pm0.08$, and is plotted in Fig. 15 as a function of W and Q^2 , along with the ZEUS measurement of exclusive J/ψ photoproduction [22]. The data is also compared to the LO calculation of Martin, Ryskin and Teubner (MRT) [23] with three different gluon distributions: MRST02 [24], CTEQ6M [25] and ZEUS-S [15], obtained from NLO DGLAP analyses of structure function data and normalized to the ZEUS photoproduction measurement at $W=90 \ {\rm GeV}$. While CTEQ6M de-

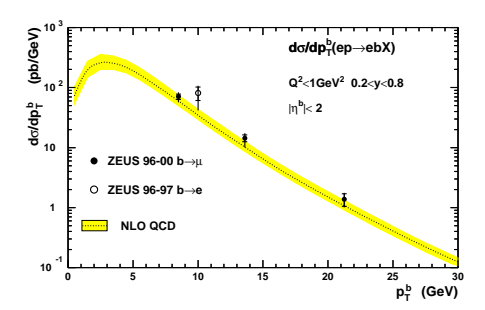


Figure 13. Differential cross section for b-quark production as a function of the b-quark transverse momentum p_T^b for b-quark pseudorapidity $|\eta^b| < 2$ and for $Q^2 < 1$ GeV², 0.2 < y < 0.8. The filled points show the new ZEUS results and the open point is the previous ZEUS measurement in the electron channel [18]. The full error bars are the quadratic sum of the statistical (inner part) and systematic uncertainties. The dashed line shows the NLO QCD prediction with the theoretical uncertainty shown as the shaded band.

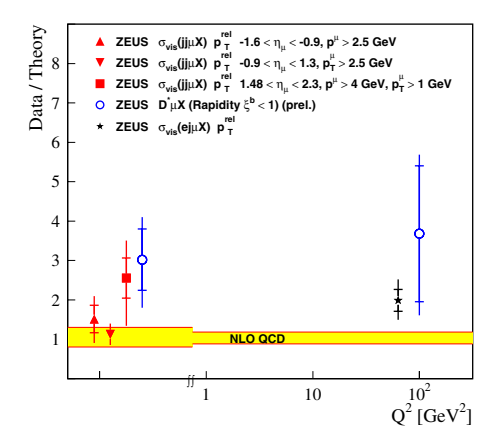


Figure 14. The ratio of ZEUS data to a NLO QCD calculation as a function of Q^2 for differential b-quark cross sections measured in photoproduction and DIS events with at least one jet reconstructed in the Breit frame and a muon. The NLO shaded band shows the uncertainty due to renormalization and factorization scales and b-quark mass.

scribes the W and Q^2 dependence of the data, MRST02 has the wrong shape in W, particularly at low Q^2 . ZEUS-S describes the W dependence but falls too quickly with increasing Q^2 . The data exhibit a strong sensitivity to the gluon distribution in the proton. However, full NLO calculations are needed in order to use these data in global fits to constrain the gluon density.

ZEUS has measured the exclusive electroproduction of ϕ mesons, $ep \to e\phi p$, for photon virtualities in the range and $2 < Q^2 < 70 \text{ GeV}^2$, for photon-proton center-of-mass energies in the range 35 < W < 145 GeV and $|t| < 0.6 \text{ GeV}^2$. Figure 16 (top) shows the extracted cross section of the process $\gamma^* p \to \phi p$ measured as a function of W and Q^2 . The data were fit to a dependence $\sigma \propto W^\delta$ with $\delta \approx 0.3$. The fit values of δ are compared to those from previous ZEUS measurements for different VM in Fig. 16 (bottom). The behavior of δ is consistent with a scaling of the W dependence for exclusive VM production with $Q^2 + M_V^2$.

ZEUS has studied whether hard diffractive processes can be factorized into universal diffractive PDFs and the partonic cross section using a data sample from 30 times the luminosity of the previous ZEUS result [26] and using a new forward detector added near the beam pipe, that allows measurements to be made over a wider kinematic range. Dijet events are selected with $0.2 < y < 0.85, Q^2 < 1.0 \text{GeV}^2, x_{pom} < 0.035, E_T^{jet1(2)} > 7.5(6.5)$ GeV and $-1.5 < \eta^{jet1,2} < 2.0$. Diffractive events are selected with a rapidity gap in the forward region, $3 < \eta < 5$. Figure 17 shows that the LO prediction from the RAPGAP [28] generator, normalized to the data by a factor of 0.59 describes the x_{γ}^{obs} well in both direct (high x_{γ}^{obs}) and resolved (low x_{γ}^{obs}) enriched regions. A reduction in the data below the prediction

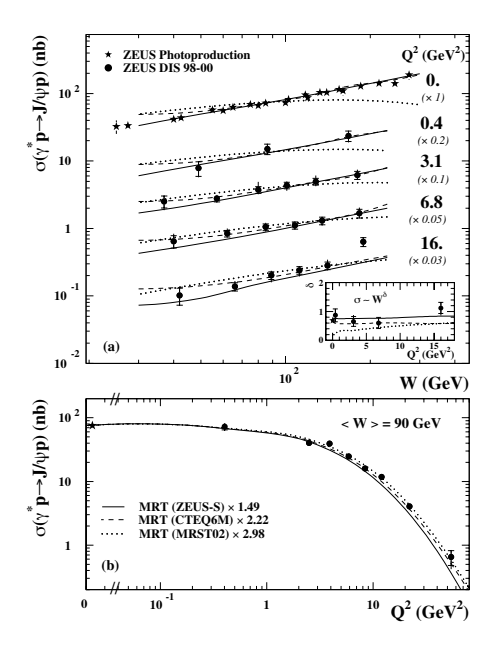


Figure 15. Exclusive J/ψ electroproduction cross section (a) as a function of W for four values of Q^2 and (b) as a function of Q^2 at $\langle W \rangle = 90$ GeV. ZEUS photoproduction results are also shown. The data are compared to the MRT predictions (see text) obtained with different parametrisations of the gluon density and normalized to the ZEUS photoproduction point at $\langle W \rangle = 90$ GeV. The insert shows the parameter δ as a function of Q^2 . The inner error bars represent the statistical uncertainties, the outer bars are the statistical uncertainties, the outer bars are the statistical and systematic uncertainties added in quadrature. An overall normalisation uncertainty of $^{+5\%}_{-8\%}$ was not included.

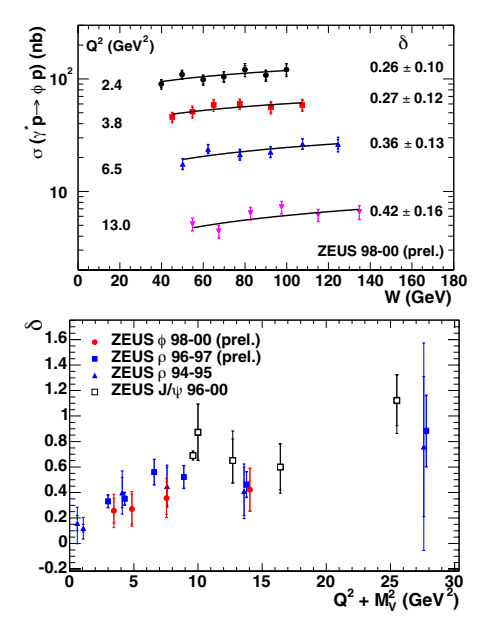


Figure 16. (top) Exclusive ϕ cross section as a function of W for four values of Q^2 . The solid lines are a result of a fit to the form $\sigma \propto W^{-\delta}$. (bottom) Extracted values of δ compared with results from other VMs. The inner error bars represent the quadratic sum of the statistical uncertainties, while the outer bars represent the quadratic sum of the statistical and systematic uncertainties. The overall normalization uncertainty of $^{+10.4}_{-6.6}\%$ is not included in the error bar in the upper plot.

at lower x_{γ}^{obs} would suggest a suppression of the resolved photon processes with respect to the direct photon processes, indicating a breakdown of QCD factorization, but this is not observed.

ZEUS has studied CC DIS events with a Large Rapidity Gap (LRG) for $Q^2 > 200 \text{GeV}^2$ and $x_{Bj} > 0.05$. Figure 18 shows the distribution of η_{max} , where η_{max} is the pseudorapidity of the energy distribution in the calorimeter above 400 MeV which is closest to the outgoing proton direction. The data are compared with a combination of non-diffractive events produced by DJANGOH [27] interfaced to ARIADNE [11] for fragmentation and diffractive events modeled by the RAPGAP [28] generator. The upper plot in Fig. 18 shows an excess of events with a LRG over ARIADNE at low η_{max} . The bottom plot in Fig. 18 shows the η_{max} distribution with the requirements that the Forward Plug Calorimeter (extending

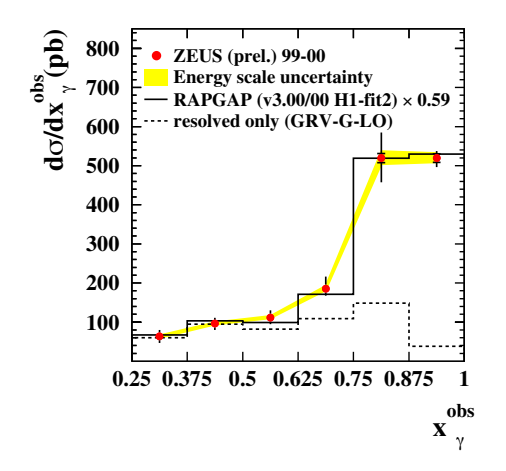


Figure 17. The single differential cross section in x_{γ}^{obs} . The data is shown as dots with the corresponding energy scale uncertainty shown as a band; the inner error bards indicate the statistical uncertainty and the outer error bars indicate the statistical and systematic errors added in quadrature. The solid lines show the prediction of the LO RAPGAP MC, normalized to the data by a factor of 0.59; the dashed line is the resolved photon component from RAPGAP

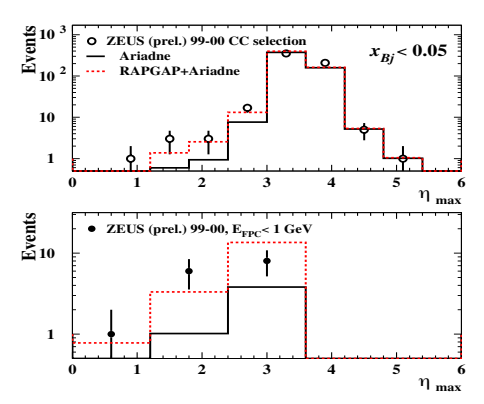


Figure 18. (top) η_{max} distribution for ZEUS CC DIS data (dots), the non-diffractive ARIADNE and ARIADNE plus RAPGAP and (bottom) the same plot with the additional $E_{FPC} < 1$ cut.

the acceptance of the forward calorimeter by one unit to $\eta=5$) satisfies $E_{FPC}<1$ GeV, suppressing the non-diffractive contribution. Additional cuts of $\eta_{max}<2.9$ and $x_{pom}<0.05$ (where x_{pom} is the fraction of proton longitudinal momentum carried by the diffractive exchange) further reduce the non-diffractive background, resulting in 9 data events, 5.6 ± 0.7 diffractive CC (RAPGAP) simulated events and 2.1 ± 0.4 non-diffractive CC (ARIADNE) simulated events.

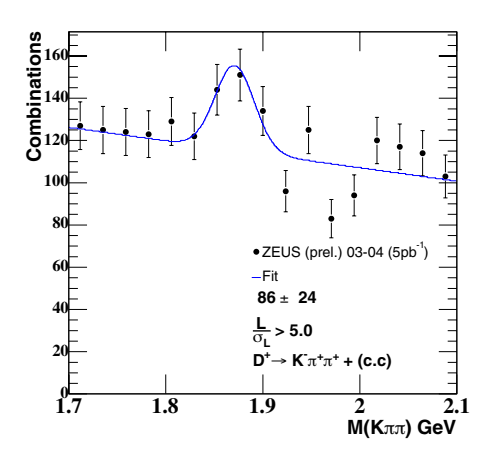
The assumption that the excess of LRG events over the non-diffractive expectation from ARIADNE is due to diffraction results in the cross section, $\sigma^{CC\ DIFF}_{(Q^2>200GeV^2,x_{pom}<0.05)}=0.49\pm0.20(stat.)\pm0.13(syst.)$ pb, compared with a prediction of 0.4 pb from RAPGAP. The ratio of diffractive to total CC cross sections,

$$\sigma_{(Q^2>200GeV^2,x_{pom}<0.05)}^{CC\ DIFF}\Big/\sigma_{(Q^2>200GeV^2,x_{Bj}<0.05)}^{CC\ TOT}=\left(2.9\pm1.2\left(stat\right)\pm0.8\left(syst\right)\right)\%,$$

is similar to that measured in the NC DIS process [29] in a similar kinematic region.

6 HERA-II Results

Since the start of HERA-II running, ZEUS has been recording the collisions of polarized positrons with protons using its new microvertex and forward tracking detectors. Figure 19 shows use of the new microvertex detector to place a significance cut on a secondary vertex to extract a D^+ sample from 5 pb⁻¹ of HERA-II



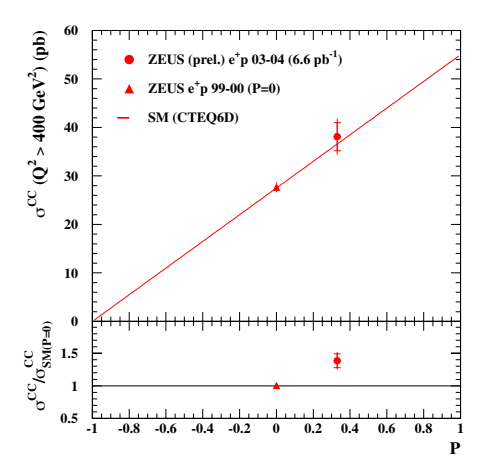


Figure 19. D^+ signal extracted from HERA-II data using the new ZEUS microvertex detector.

Figure 20. Polarized and unpolarized CC DIS cross sections compared with SM predictions.

data.

Figure 20 shows the ZEUS measurement of the polarized CC DIS cross section for $Q^2 > 400 {\rm GeV}^2$ from 6.6 pb⁻¹ of HERA-II luminosity with 33% polarized positrons. The systematic error of about 2% is principally due to the calorimeter energy scale, the event selection, PDF uncertainty and the trigger acceptance. Also plotted is the ZEUS HERA-I unpolarized point [2] and the SM prediction using the CTEQ6M [3] PDF. Both data points are shown to be consistent with the SM and the polarized positron CC cross section has been measured, $\sigma_{CC} = 38.1 \pm 2.9 (stat.) \pm (sys.) \pm 2.0 (lumi.) \pm (pol)$ pb.

7 Summary and Conclusions

New results from ZEUS are completing the picture from HERA-I. These include the full complement of structure function and cross section measurements. Precise jet measurements have determined α_s within 2% and are being used to constrain the structure function QCD fits. A new era in hadron spectroscopy has begun with the evidence of pentaquark states. Charm physics is now providing new constraints on the gluon distribution in the proton. DIS and photoproduction b cross sections are now in general agreement with NLO QCD calculations. There is also new understanding of diffraction in terms of QCD calculations.

The first ZEUS results from HERA-II show great promise with new charm data with the new ZEUS microvertex detector and the measurement of the polarized CC DIS cross section. These provide just a taste of the rich physics harvest to follow.

References

 A.M. Cooper-Sarkar, R.C.E. Devenish and A. De Roeck, Int. J. Mod. Phys. A 13, 3385 (1998).

- 2. ZEUS Collab., S. Chekanov et al., "High- Q^2 neutral current cross sections in e^+p deep inelastic scattering at $\sqrt{s}=318$ -GeV," arXiv:hep-ex/0401003. ZEUS Collab., S. Chekanov et al., Eur. Phys. J. C **28**, 175 (2003). ZEUS Collab., S. Chekanov et al., Eur. Phys. J. C **21**, 443 (2001). ZEUS Collab., J. Breitweg et al., Eur. Phys. J. C **11**, 427 (1999).
- 3. S. Kretzer, H. L. Lai, F. I. Olness and W. K. Tung, JHEP 7, 12 (2002).
- 4. V. N. Gribov and L. N. Lipatov, Sov. J. Nucl. Phys. 15, 438 (1972).
 - V. N. Gribov and L. N. Lipatov, Sov. J. Nucl. Phys. 15, 675 (1972).
 - Yu.L. Dokshitzer, Sov. Phys. JETP 46, 641 (1977).
 - G. Altarelli and G. Parisi, Nucl. Phys. B 126, 298 (1977).
- 5. Y. L. Dokshitzer and B. R. Webber, Phys. Lett. B 352 (1995) 451.
- M. Dasgupta and G. P. Salam, Eur. Phys. J. C 24 (2002) 213.
- 7. Z. Nagy and Z. Trocsanyi, Phys. Rev. Lett. 87, 082001 (2001).
- 8. A. D. Martin et al., Eur. Phys. J. C23 (2002) 73.
- 9. G. Ingelman et al., Comp. Phys. Comm. 101, 108 (1997).
- 10. A. H. Mueller, Nucl. Phys. Proc. Suppl. C18 125 (1991).
- L. Lönnblad, Comp. Phys. Comm. 71 15 (1992); L. Lönnblad, Z. Phys. C 65, 285 (1995).
- S. Catani and M. H. Seymour, Nucl. Phys. B 485, 291 (1997); Erratum in Nucl. Phys. B 510, 503 (1998).
- 13. ZEUS Collaboration, S. Chekanov *et al.*, DESY-04-056 hep-ex/0403051, Phys. Lett. B (in press).
- 14. DIANA Collaboration, V.V. Barmin et al., Phys. Atom. Nucl. 66 (2003) 1715; A.E. Asratyan, A.G. Dolgolenko, M.A. Kubantsev, Preprint hep-ex/0309042, 2003; SVD Collaboration, A. Aleev et al., Preprint hep-ex/0401024, 2004; HERMES Collaboration, A. Airapetian et al., Phys. Lett. B 585 (2004) 213; COSY-TOF Collaboration, M. Abdel-Bary et al., Preprint hep-ex/0403011, 2004.
- 15. ZEUS Coll., S. Chekanov et al., Phys. Rev. **D67** (2003) 012007.
- 16. H1 Coll., C. Adloff et al., Phys. Lett. **B528** (2002) 199.
- 17. ZEUS Coll., J. Breitweg *et al.*, Eur. Phys. J. **C12** (2000) 35.
- 18. ZEUS Coll., J. Breitweg et al., Eur. Phys. J. C18 (2001) 625.
- 19. ZEUS Coll., S. Chekanov et al., DESY Preprint DESY-03-212, 2003.
- 20. S. Frixione et al., Nucl. Phys. **B412** (1994) 225.
- 21. B.W. Harris and J. Smith, Phys. Rev. **D57** (1998) 2806.
- 22. ZEUS Coll., S. Chekanov et al., Eur. Phys. J. C 24 (2002) 345.
- 23. A.D. Martin, M.G. Ryskin and T. Teubner, Phys. Rev. **D** 62 (2000) 14022.
- 24. A.D. Martin et al., Eur. Phys. J. C 23 (2002) 73.
- 25. J. Pumplin et al., JHEP **0207** (2002) 012.
- 26. ZEUS Coll., S. Chekanov et al., Eur Phys. J. C 5 (1998) 41.
- 27. H. Spiesberger, www.desy.de/hspiesb/heracles.html (1998).
- 28. H. Jung, Comp. Phys. Comm. **86** (1995) 147.
- 29. ZEUS Coll., J. Breitweg et al., Eur. Phys. J. C 6 (1999) 43.